Journal of the Nigerian Association of Mathematical Physics
Volume 60 **(April – June** *2021 Issue***), pp35 –50**

UNSTEADY MHD DOUBLE DIFFUSIVE FLOW OF CASSON FLUID PAST STRETCHING SHEET EMBEDDED IN A POROUS MEDIUM WITH VARIABLE THERMO-PHYSICAL PROPERTY AND NANO-PARTICLES

[1] Sogbetun L. O., [2]Fasasi Y. A., [3]Akinosho G. A. and [4]Ogunbade A.O.

[1,3,4]Department of Computer Science, Federal College of Animal Health and Production Technology, Moor Plantation, Ibadan.
[2]Department of Mathematics and Statistics, The Oke-Ogun Polytechnic, Saki.

Abstract

This work examines influence of temperature dependent plastic dynamic viscosity and thermal conductivity flow on Casson nanofluid in the presence of magnetic field. The flow is induced by both unsteady linearly stretching sheet placed inside a porous medium and buoyancy effects which are generated by the temperature difference between the dissolved species and space dependent internal heat generation. Variable viscosity and thermal conductivity of the fluid assume linear functions of temperature. The governing partial differential equations are reduced to coupled ordinary differential equations by employing suitable transformations and later solved numerically. It is observed that an increase in local unsteadiness parameter reduces fluid velocity, temperature and concentration. Effects of other relevant physical parameters on fluid velocity, temperature and concentration distribution as well as on the wall shear stress, heat and mass transfer rates are carefully explained.

Keywords**:** Casson nanofluid; Variable viscosity; Variable thermal conductivity; Buoyancy effect; Porous medium; Wall shear stress; Wall shear heat; Heat and mass transfer;

Introduction

Work on significance of boundary layer flow over a stretching surface abound in literature. In plentiful engineering operations, its applications are found, in cooling bath, extraction of continuous casting, wire coating, aerodynamic extrusion, metallurgical process, glass blowing, manufacturing of rubber and plastic sheets, crystal growing, and so on. The procedure adopted for heat transfer and stretching of sheets during manufacturing of the aforementioned items plays a vital role on the quality of the final products as revealed by numerous researchers. [1] studied two-dimensional flow over continuous stretched surface employing suitable similarity transformations and numerical technique. [2] and [3] investigated viscous flow over quadratic stretching sheet. [4] and [5] examined the heat and mass transfer characteristics in boundary layer flow over exponentially stretching sheet. Combined heat transfer effects in two-dimensional incompressible flow of viscous fluid cause due to nonlinearly stretching sheet was analysed by [6], [7] and [8].

However, all the aforementioned research work investigated different cases of steady stretching sheet. In practice, the stretching sheet is most likely to be unsteady due to the abrupt variation in wall velocity, free stream or wall temperature etc. Consequently, the flow field, heat and mass transfer are suitably described as function of time. [9] investigated unsteady flow due to stretching sheet. Further, significance of variable wall temperature and variable heat flux in boundary layer flow over unsteady stretching surface using similarity transformations was examined by [10]. [11] analysed influence of thermal radiation on mixed convection flow of viscous fluid induced due to unsteady stretching sheet embedded in a porous medium. [12] in his research, investigated effects of suction/injection on unsteady free convection flow of Newtonian fluid due to stretching sheet in the presence of chemical reaction. Influence of slip condition on unsteady stagnation point flow of viscous fluid caused by stretching sheet was analysed by [13].

Of concern in this work is the study of heat and mass transfer flow under the influence of magnetohydrodynamic (MHD)

Corresponding Author**:** Sogbetun L.O., Email: mailbayo2000@yahoo.co.uk, Tel: +2348038179124

and chemical reaction. Numerous studies reveal its relevance in chemical industry, cooling of nuclear reactors, MHD power generation, MHD pumps, packed-bed catalytic reactor, formation and dispersion of fog, high speed plasma, cosmic jets, enhanced oil recovery, distribution of temperature and moisture over agriculture fields, cooling of nuclear reactors, manufacturing of ceramics, underground energy transport, food processing and cooling towers, etc. [14] studied the effect of chemical reaction on boundary layer flow over a stretching sheet under the influence of magnetic field. The result of the research revealed that magnetic field improves the skin friction greatly. [15] in his work, examined hydromagnetic mixed convection flow along the wedge in the presence of suction and injection. [16] analysed the effect of thermal radiation and chemical reaction on unsteady free convection flow generated due to stretching sheet in the presence of magnetic field.
[17] employed similarity transformation to analyse influence of first order chemical reaction on the unsteady boundary layer flow of electrically conducting fluid caused by stretching sheet. [18] investigated hydrodynamic slip effect on electrically conducting flow past a stretching sheet. Further, [19] examined heat and mass transfer flow of hydromagnetic boundary layer flow towards stretching sheet in the presence of chemical reaction. [20], [21] and [22] in a separate work studied the influence of magnetic field on two-dimensional flow of nanofluid with and without slip condition. [23] again examined two dimensional electrically conducting
flow of nanofluid due to stretching sheet under the influence of convective boundary condition.
Effect of first order chemical reaction on two-dimensional flow of viscous fluid in the presence and absence of magnetic field was also studied by [24]and [25]. In a separate work, [26] again investigated the influence of thermal radiation on viscous flow of micropolar nanofluid in the presence of magnetic field.
Plethora applications of non-Newtonian fluids in several industrial processes have been established in research work. Its multiplicity significance in: design of solid matrix heat, nuclear waste disposal, chemical catalytic reactors, geothermal energy production, ground water hydrology, transpiration cooling, petroleum reservoirs and so on have been widely reported. Non-Newtonian fluid deviates from the Newtonian's law of viscosity, relationship between stress and strain rate is nonlinear and this makes the fluids more complex when compare to Newtonian fluids. Scientists have proposed quite a few models for the study of non-Newtonian fluids, but none of these models developed can completely describe all the properties exhibit by non-Newtonian fluids. Casson fluid, a shear thinning fluid is a special class of non-Newtonian fluids which is presumed to have an infinite viscosity at zero rate of shear, a yield stress below which no flow occurs and a zero viscosity at an infinite rate of shear. Typical examples of Casson fluid are honey, jelly, tomato sauce, concentrated fruit juices, etc. The Casson model, also refers to as rheological model was initially formulated by [27] for viscous suspension of cylindrical particles and is the most appropriate rheological model for blood and chocolate. In addition, Casson fluid has yield stress and great importance in polymer processing industries and biomechanics. [28] studied the influence of thermal radiation on unsteady flow of Casson fluid caused by stretching sheet subjected to suction/blowing. [29] investigated the three-dimensional hydromagnetic flow of Casson fluid in a porous medium. [30] obtained numerical solutions of electrically conducting slip flow of Casson Nanofluid generated during stretching sheet under the influence of convective boundary condition by means of similarity transformations. Benazir et al. [31] investigated unsteady Casson flow through a vertical cone and flat sheet in the presence of magnetic field. In recent times, [32] examined unsteady electrically conducting flow of Casson Nanofluid under of slip and convective boundary conditions.
This paper extends the work of [33]by examining the influence of variable plastic dynamic viscosity and thermal conductivity on unsteady electrically conducting flow of Casson Nanofluid towards linearly stretching sheet saturated in a porous medium. The highly nonlinear partial differential equations are transformed into coupled ordinary differential equations using suitable similarity transformations and then solved numerically using Runge-Kutta Gill technique (a modified version of classical Runge-Kutta method). Numerical analysis includes effects of pertinent variables on the fluid flow, thermal field and nanoparticle concentration are made and discussed.

Mathematical Formulation

Consider MHD boundary layer flow of Casson fluid past an unsteady linearly stretching sheet through porous medium under the influence of variable thermo-physical property and nanoparticles. The x- axis is chosen along the direction of stretching sheet and y- axis is normal to the surface. The flow of heat and mass transfer starts at $t = 0$. The sheet is pulled out of the slit at the origin $(x = 0, y = 0)$ and moves with velocity $U_w(x,t) = ax/(1-\alpha t),\ a > 0, \alpha \geq 0$ are constants, and a is the initial stretching rate. Further, a constant magnetic field B_0 is applied normally to the stretching sheet. As the fluid pressure is constant throughout the boundary, it is assumed that induced magnetic field is small in comparison to the applied magnetic field; hence it is neglected. Following [34], the rheological equation of an isotropic and incompressible flow of a Casson fluid is expressed as

$$\tau_{ij} = \begin{cases} 2\left(\mu_B + \dfrac{P_y}{\sqrt{2\pi}}\right)e_{ij}, & \pi > \pi_c \\ 2\left(\mu_B + \dfrac{P_y}{\sqrt{2\pi_c}}\right)e_{ij}, & \pi < \pi_c \end{cases} \tag{1}$$

$$P_y = \frac{\mu_b\sqrt{2\pi}}{\beta} \tag{2}$$

where P_y is the yield stress of the fluid, μ_b the plastic dynamic viscosity of the non-Newtonian fluid, π the product of the component of deformation rate with itself (i.e. $\pi = e_{ij}e_{ij}$), e_{ij} the (i, j)th component of the deformation rate and π_c the critical value based on the non-Newtonian model. The temperature and concentration at the sheet are T_w and C_w respectively while T_∞ and C_∞ are respectively the ambient conditions. It is assumed that both temperature T_w and concentration C_w at the surface vary with distance from the origin and time are therefore given as in [35] by

$$T_w(x,t) = T_\infty + \frac{bx}{(1-\alpha t)^2}, \qquad C_w(x,t) = C_\infty + \frac{cx}{(1-\alpha t)^2} \tag{3}$$

where b and c are constants. The surface temperature and surface concentration increase if b and c are positive and reduce if they are negative from T_∞ and C_∞ at the origin to x and the temperature and concentration increase/decrease along the sheet. The expressions $U_w(x,t), T_w(x,t)$ and $C_w(x,t)$ are only valid for $t < \alpha^{-1}$ but not when $\alpha = 0$. Under the usual boundary layer and Boussinesq's approximation, the governing equations of Casson nanofluid along with continuity equation are given as

$$\frac{\partial u}{\partial x} + \frac{\partial v}{\partial y} = 0 \tag{4}$$

$$\frac{\partial u}{\partial t} + u\frac{\partial u}{\partial x} + v\frac{\partial u}{\partial y} = \frac{1}{\rho}\left(1+\frac{1}{\beta}\right)\frac{\partial}{\partial y}\left(\mu_B(T)\frac{\partial u}{\partial y}\right) - \left(\frac{\sigma B_0^{\,2}}{\rho} + \frac{\vartheta_B(T)\varphi}{k_1}\right)u \pm g\beta_T(T-T_\infty) \pm g\beta_C(C-C_\infty) \tag{5}$$

$$\frac{\partial T}{\partial t} + u\frac{\partial T}{\partial x} + v\frac{\partial T}{\partial y} = \frac{1}{\rho c_p}\frac{\partial}{\partial y}\left(k(T)\frac{\partial T}{\partial y}\right) + \tau\left(D_B\frac{\partial C}{\partial y}\frac{\partial T}{\partial y} + \frac{D_T}{T_\infty}\left(\frac{\partial T}{\partial y}\right)^2\right) - \frac{1}{\rho c_p}\frac{\partial q_r}{\partial y} + \left(1+\frac{1}{\beta}\right)\frac{\vartheta_B(T)}{c_p}\left(\frac{\partial u}{\partial y}\right)^2 \tag{6}$$

$$+ \frac{\sigma B^2(x,t)}{\rho C_p}u^2 + \frac{Q_0}{\rho C_p}(T-T_\infty)$$

$$\frac{\partial C}{\partial t} + u\frac{\partial C}{\partial x} + v\frac{\partial C}{\partial y} = D_B\frac{\partial^2 C}{\partial y^2} + \frac{D_T}{T_\infty}\frac{\partial^2 T}{\partial y^2} - k_c(C-C_\infty) \tag{7}$$

where ϑ is kinematic viscosity of Casson fluid, $\beta = \mu_\beta\sqrt{2\pi_c}/P_y$ is the non-Newtonian Casson parameter, K is the permeability of the porous medium, σ is the electrical conductivity, B_0 is the strength of the magnetic field, ρ is the density of the Casson fluid, D is the diffusion coefficient of species in the fluid, α_0 is the thermal diffusivity, and $k(t) = k_0/(1-\alpha t)\,k(t)$ is the time dependent reaction rate, where $k > 0$ represents destructive reaction, $k < 0$ represents constructive reaction, and k_0 is a constant. The boundary conditions are given as

$$u = U(x,t), \qquad v = 0 \qquad T = T_w(x,t), \qquad C = C_w(x,t), \qquad y = 0 \tag{8a}$$

$$u \to 0, \qquad T \to T_\infty, \qquad C \to C_\infty, \qquad y \to \infty \tag{8b}$$

By using Rosseland approximation, the radiative heat flux, q_r takes the form [36], [37] as

$$q_r = \frac{-4\sigma}{3k^*}\frac{\partial T^4}{\partial y}, \tag{9}$$

where σ is the Stefan–Boltzmann constant and k^* is the absorption coefficient. T^4 may be expressed as a linear function of the freestream temperature T_∞. Expanding T^4 in a Taylor series about T_∞ and neglecting higher order terms, we can write

$$T^4 \approx T_\infty^4 + 4T_\infty^3 T - 4T_\infty^3 T_\infty \tag{10}$$

Incorporating equations (9) and (10) in equation (5) gives

$$\frac{\partial T}{\partial t} + u\frac{\partial T}{\partial x} + v\frac{\partial T}{\partial y} = \frac{1}{\rho c_p}\frac{\partial}{\partial y}\left(k(T)\frac{\partial T}{\partial y}\right) + \tau\left(D_B\frac{\partial C}{\partial y}\frac{\partial T}{\partial y} + \frac{D_T}{T_\infty}\left(\frac{\partial T}{\partial y}\right)^2\right) + \frac{16\sigma T_\infty^3}{3k^*\rho c_p}\frac{\partial^2 T}{\partial y^2} + \left(1+\frac{1}{\beta}\right)\frac{\vartheta_B(T)}{c_p}\left(\frac{\partial u}{\partial y}\right)^2 \tag{11}$$

$$+ \frac{\sigma B^2(x,t)}{\rho C_p}u^2 + \frac{Q_0}{\rho C_p}(T - T_\infty)$$

It is assumed that the plastic dynamic viscosity of non-Newtonian fluid and its thermal conductivity are linear function of temperature as stated in [38], we have

$$\mu_B(T) = \mu_B^*(1 + b_1(T_w - T)), \qquad k(T) = k^*(1 + \delta(T - T_\infty)) \tag{12}$$

Now introduce the following transformations (13)

$$u = \frac{\partial \psi}{\partial y}, \quad v = -\frac{\partial \psi}{\partial x}, \qquad \eta = \sqrt{\frac{a}{\vartheta_B(1-\alpha t)}}y, \quad \psi = \sqrt{\frac{\vartheta_B a}{1-\alpha t}}xf(\eta), \quad \theta = \frac{T - T_\infty}{T_w - T_\infty}, \quad \phi = \frac{C - C_\infty}{C_w - C_\infty} \tag{13}$$

Equations (4),(5),(7),(8) and (12) take the form (14) – (17):

$$\left(1+\frac{1}{\beta}\right)(1+\xi(1-\theta))f''' - \left(1+\frac{1}{\beta}\right)\xi\theta' f'' + ff'' - f'^2 - \frac{A}{2}\left(2f' + \eta f''\right) - \left(K(1+\xi(1-\theta)) + M^2\right)f' + \lambda(\theta + N\phi) = 0 \tag{14}$$

$$\left((1+\varepsilon\theta) + \frac{4}{3}R_d\right)\theta'' + (\varepsilon + P_r N_t)\theta'^2 + P_r f\theta' + P_r N_b^*\phi'\theta' - P_r f'\theta + P_r E_c(1+\xi(1-\theta))\left(1+\frac{1}{\beta}\right)f''^2 + P_r E_c M f'^2 + P_r Q\theta \tag{15}$$

$$- P_r\frac{A}{2}(\eta\theta' + 4\theta) = 0$$

$$\phi'' + Lef\phi' - Lef'\phi + \frac{N_t}{N_b}\theta'' - \frac{A}{2}Le(4\phi + \eta\phi') - RLe\,\phi = 0 \tag{16}$$

$$f(0) = 0, \qquad f'(0) = 1, \qquad \theta(0) = 1, \qquad \phi(0) = 1 \tag{17a}$$

$$f'(\infty) \to 0, \qquad \theta(\infty) \to 0, \qquad \phi(\infty) \to 0 \tag{17b}$$

Where ξ is the variable plastic dynamic viscosity parameter, ε is the variable thermal conductivity parameter, K is the porosity parameter, M is the magnetic parameter, A is the local unsteadiness parameter, $\lambda = \pm\frac{Gr_x}{\mathrm{Re}_x^2}$ is the thermal buoyancy parameter ($\lambda > 0$ corresponds to assisting flow, $\lambda = 0$ indicates no convection and $\lambda < 0$ denotes the opposing flow) (Gr_x and Re_x being Grashof number and local Reynold number respectively), N is the buoyancy ratio parameter, P_r is the Prandtl number, R_d is the radiation parameter, E_c is the Eckert number, Q, is the internal heat generation N_t is the thermophoretic parameter, N_b^* is the diffusion parameter, L_e is the Lewis number, and R is the chemical reaction parameter and are defined as [38]

$$K = \frac{\vartheta_B\varphi(1-\alpha t)}{ak_1}, \quad M = \frac{\sigma B_0^2(1-\alpha t)}{\rho a}, \quad A = \frac{\alpha}{a}, \quad G_{rx} = \frac{g\beta_\tau(T_w - T_\infty)x^3}{\vartheta_B^2}, \quad N = \frac{\beta_c(C_w - C_\infty)}{\beta_T(T_w - T_\infty)},$$

$$N_t = \tau\frac{D_T}{T_\infty}\left(\frac{T_w - T_\infty}{\vartheta_B}\right), \quad N_b^* = \frac{\tau D_B}{\vartheta_B}(C_w - C_\infty), \quad \mathrm{Re}_x = \frac{xU_w}{\vartheta_B}, \quad P_r = \frac{\mu c_p}{k}, \lambda = \pm\frac{Gr_x}{\mathrm{Re}_x^2}, Gr_x = \frac{g\beta_T(T_w - T_\infty)x^3}{\vartheta^2}, \quad R_d = \frac{4\sigma^* T_\infty^3}{kk^*},$$

$$Ec = \frac{a^2x^2}{(T_w - T_\infty)c_p(1-\alpha t)^2}, \quad Q = \frac{(1-\alpha t)Q_0}{a\rho c_p}, \quad Le = \frac{\vartheta_B}{D_B}\ R = \frac{(1-\alpha t)k_c}{a}, \quad \varepsilon = \delta(T_w - T_\infty), \quad \xi = b_1(T_w - T_\infty), \quad \beta = \frac{\mu_b\sqrt{2\pi}}{p_y}$$

The wall skin friction, wall heat flux, and wall mass flux are represented as follows:

$$\tau_w = \left(\mu_B(T)\left(1+\frac{1}{\beta}\right)\frac{\partial u}{\partial y}\right)_{y=0}, \quad q_w = -\left(\left(\alpha_1 + \frac{16\sigma^* T_\infty^3}{3k_1^*}\right)\frac{\partial T}{\partial y}\right)_{y=0} \text{ and } J_w = -D_B\left(\frac{\partial C}{\partial y}\right)_{y=0} \tag{18}$$

The dimensional skin friction coefficient, the local Nusselt number and local Sherwood number on the surface along $x-$ direction are respectively defined as,

$$Cf_x = \frac{\tau_w}{\rho u_w^2},\ Nu_x = \frac{xq_w}{\alpha_1(T_w - T_\infty)} \text{ and } Sh_x = \frac{xJ_w}{D_B(C_w - C_\infty)} \tag{19}$$

Incorporating equations (13) and (18) in (19), the corresponding dimensionless forms give

$$(\mathrm{Re}_x)^{1/2} Cf_x = \left(1 + \frac{1}{\beta}\right)(1 + \xi(1 - \theta(0)))f''(0), \qquad (\mathrm{Re}_x)^{-1/2} Nu_x = -\left((1 + \varepsilon\theta(0)) + \frac{4}{3}R_d\right)\theta'(0) \tag{20}$$

$$(\mathrm{Re}_x)^{-1/2} Sh_x = -\phi'(0) \tag{21}$$

Numerical Scheme

The solution of the nonlinear governing equations (14) – (16) along with associated boundary conditions in equation (17) are obtained via Runge-Kutta Gill technique. The order analysis, consistency analysis and stability analysis show that Runge-Kutta Gill is order four, stable and consistent [39]. The boundary layer thickness η_∞ and step size h are cautiously chosen to satisfy the boundary conditions $f'(\eta = \infty), \theta(\eta = \infty), \phi(\eta = \infty)$ and desired accuracy of an error tolerance of 10^{-6}.

Results and Discussion

The following discussion centres around analyzing the influence of some controlling parameters on the problem examines in this journal. Thus, graphical representations of the effect of the local unsteadiness (A), variable plastic dynamic viscosity parameter (ξ), variable thermal conductivity parameter (ε), Casson fluid parameter (β), magnetic parameter (M), porosity parameter (K), thermal buoyancy parameter (λ), buoyancy ratio parameter (N), radiation parameter (R_d), Eckert number (E_c), internal heat generation (Q), thermophoretic parameter (N_t), diffusion parameter (N_b), Lewis number (L_e) and chemical reaction parameter (R) on the fluid velocity $(f(\eta))$, temperature $(\theta(\eta))$ and concentration $(\phi(\eta))$ profile are adequately explained.

Also examine is the variation of skin friction, the local Nusselt number and the Sherwood number with some of the aforementioned controlling parameters.

Table 1 Values of dimensionless skin friction, local Nusselt number and Sherwood number when $Ec = 0.2, R = 0.2, P_r = 0.72, Q = 0.2, N = 0.6, R_d = 0.6 \xi = 0.8, \varepsilon = 0.8, A = 0.5, \beta = 0.8,$ $\lambda = 0.4, M = 0.4, L_e = 0.62, N_t = 0.2, N_b = 0.6$ and $K = 0.5$ except when stated otherwise

ξ	ε	A	β	λ	M	L_e	N_t	N_b	K	$\left(1+\frac{1}{\beta}\right)f''(0)$	$-\left(1+\frac{4}{3}R_d\right)\theta'(0)$	$-\phi'(0)$
0.8	0.8	0.5	0.8	0.4	0.4	0.62	0.2	0.6	0.5	-1.9864	0.9525	1.1061
5.0										-3.0289	0.8669	1.0953
	5.0									-1.8620	0.5591	1.1478
		1.5								-2.5148	1.4338	1.4802
			5.0							-1.3697	0.9440	1.0820
				1.0						-1.4635	1.0003	1.1246
					2.0					-3.5353	0.7592	1.0660
						2.57				-2.0326	0.9147	2.4386
							1.5			-1.9328	0.8778	0.8024
								5		-1.9021	0.5372	1.1645
									2	-2.7826	0.8664	1.0776

The impact of $\xi, \varepsilon, A, \beta, \lambda, M, L_e, N_t, N_b$ and K on the dimensionless skin friction, local Nusselt number and Sherwood number is presented in table 1. The results are in good agreement with most of the finds in the literature.

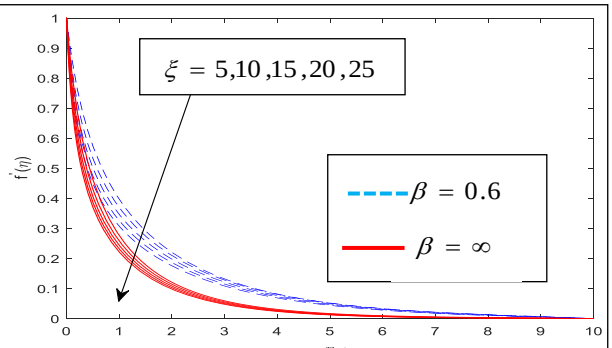

Fig. 1: Velocity profile for different values of ξ and β at

$E_c = 0.4, L_e = 0.62, R = 0.5, P_r = 0.72, Q = 0.4, \lambda = 0.4, A = 1.5$

$N = 0.8, M = 0.4, N_b = 0.4, R_d = 0.4, N_t = 0.2, K = 0.5$ and $\varepsilon = 0.8$

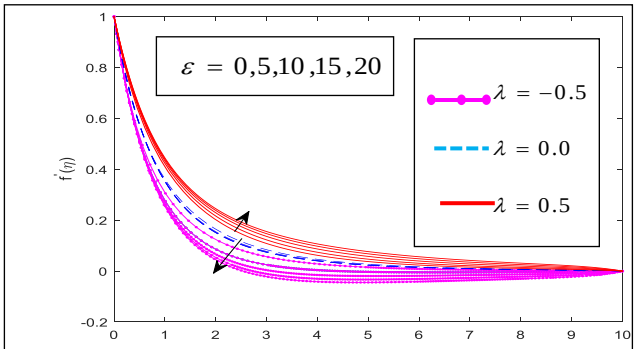

Fig. 2:Velocity profile for different values of ε and λ at

$E_c = 0.4, L_e = 0.62, R = 0.5, P_r = 0.72, Q = 0.4, A = 1.5, \beta = 0.8,$

$M = 0.4, N_t = 0.2, A = 1.5, N_b = 0.4, R_d = 0.4, K = 0.5, \xi = 0.8,$

and $N = 0.8$

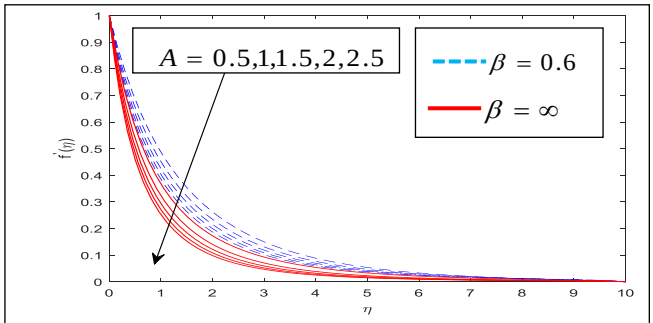

Fig.3:Velocity profile for different values of A and β at

$E_c = 0.4, L_e = 0.62, R = 0.5, P_r = 0.72, Q = 0.4, \lambda = 0.4, N = 0.8, N_t = 0.2,$

$M = 0.4, N_b = 0.4, R_d = 0.4K = 0.5, \xi = 0.8,$ vv and $\varepsilon = 0.8$

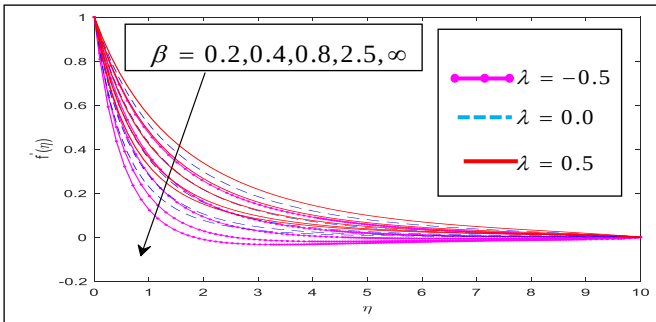

Fig. 4:Velocity profile for different values of β and λ at

$E_c = 0.4, L_e = 0.62, R = 0.5, P_r = 0.72, Q = 0.4, A = 1.5, N = 0.8, N_t = 0.2,$

$M = 0.4, N_b = 0.4, R_d = 0.4K = 0.5, \xi = 0.8,$ and $\varepsilon = 0.8$

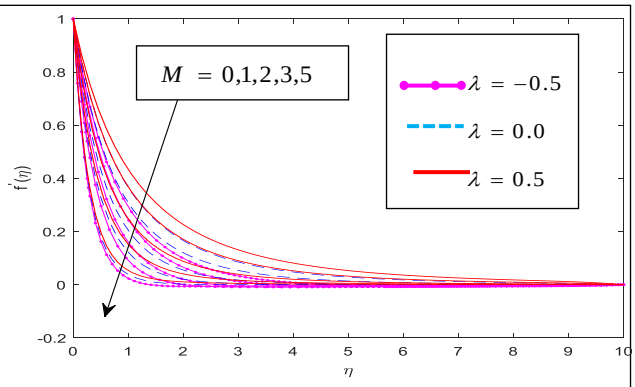

Fig. 5:Velocity profile for different values of M and λ at

$E_c = 0.4, L_e = 0.62, R = 0.5, P_r = 0.72, Q = 0.4, A = 1.5, N = 0.8, N_t = 0.2,$

$\beta = 0.8, N_b = 0.4, R_d = 0.4K = 0.5, \xi = 0.8,$ and $\varepsilon = 0.8$

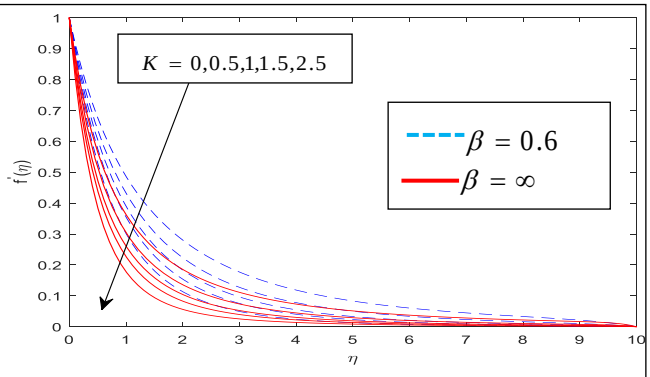

Fig. 6: Velocity profile for different values of K and A at

$E_c = 0.4, L_e = 0.62, R = 0.5, P_r = 0.72, Q = 0.4, \lambda = 0.4, N = 0.8, N_t = 0.2,$

$M = 0.4, N_b = 0.4, R_d = 0.4, A = 1.5, \xi = 0.8,$ and $\varepsilon = 0.8$

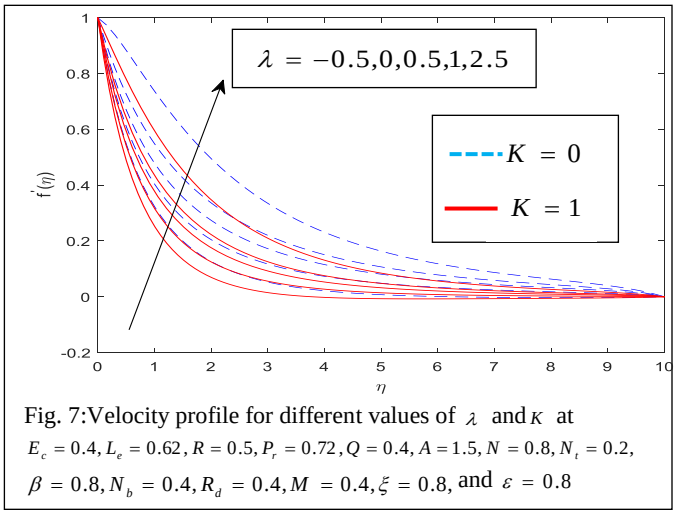

Fig. 7:Velocity profile for different values of λ and K at $E_c = 0.4, L_e = 0.62, R = 0.5, P_r = 0.72, Q = 0.4, A = 1.5, N = 0.8, N_t = 0.2, \beta = 0.8, N_b = 0.4, R_d = 0.4, M = 0.4, \xi = 0.8,$ and $\varepsilon = 0.8$

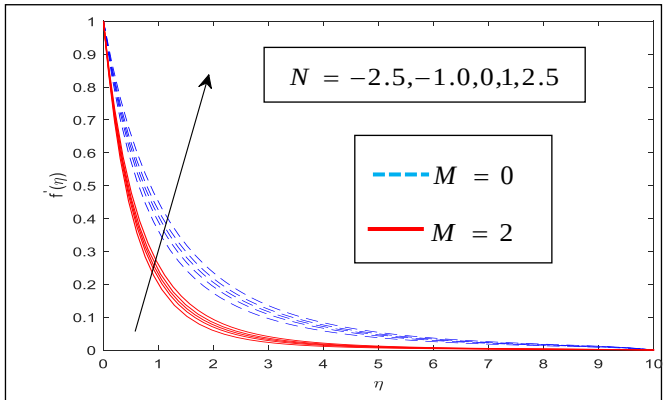

Fig. 8: Velocity profile for different values of N and M at $E_c = 0.4, L_e = 0.62, R = 0.5, P_r = 0.72, Q = 0.4, \lambda = 0.4, \beta = 0.8, N_t = 0.2, A = 1.5, N_b = 0.4, R_d = 0.4, K = 0.5, \xi = 0.8,$ and $\varepsilon = 0.8$

Figs 1-8 display profile of velocity $(f(\eta))$ for various values of $\xi, \varepsilon, A, \beta, M, K, \lambda$ and N. In Fig 1, the effect of ξ on velocity profile for $\beta = 0.6$ (Casson fluid) and $\beta = \infty$ (Newtonian fluid) is revealed. It is observed that larger values of ξ decrease the fluid velocity considerably with reduction more pronounce for the Newtonian fluid. Fig 2 exhibits effect of various values of ε on the velocity profile for different values of λ .It is noticed increasing values ε decline fluid velocity when $\lambda < 0$, has slight effect when $\lambda = 0$ and enhances when $\lambda > 0$. Fig 3 illustrates graphical representation of fluid velocity against A for $\beta = 0.6$ (Casson fluid) and $\beta = \infty$ (Newtonian fluid). It is observed that velocity reduces with increase in A for both fluids. In Fig 4 it is noticed that as β increases the fluid velocity reduces. This is because the increase in the values of β implies rise in the fluid viscosity which leads to reduction in the yield stress. Consequently, momentum boundary layer becomes thinner for larger values of β. Fig 5 portrays the variation of M on the fluid velocity for all the three cases of λ. It is clear that the velocity decreases throughout the fluid domain as values of M increases. The reduction in the fluid velocity within boundary layer may be attributed to the Lorentz force (drag-like force) produces by the magnetic field when present in an electrically conducting Casson Nano fluid. Also, a more pronounced reduction in velocity is noticed with increase in M when $\lambda < 0$. In Fig 6 the effect of K on velocity profile for $\beta = 0.6$ (Casson fluid) and $\beta = \infty$ (Newtonian fluid) is illustrated. As K increases, reduction in the momentum boundary layer thickness is observed. The explanation for this is that the holes inside porous medium become wider as K increases, hence, the fluid experiences a drag force, an opposing force in the direction of flow and consequently a reduction in the fluid velocity. Fig 7 represents the influence of λ on velocity profile for $K = 0$ and $K = 1$. It is noticed that fluid velocity increases with increase in λ. Analysis of the effect of N on fluid velocity for the presence and absence of M is displayed in Fig 8. Higher values of N increase the velocity profile. It is also realized that fluid velocity increases faster in the case of absence of magnetic parameter.

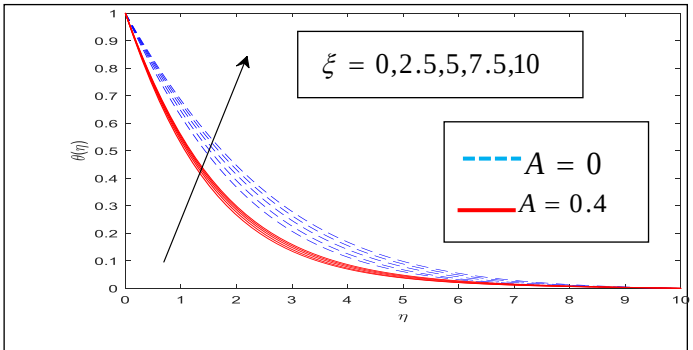

Fig.9:Temperature profile for different values of ξ and A at $E_c = 0.02, L_e = 0.62, R = 0.2, P_r = 0.72, R_d = 1.2, Q = 0.2, M = 0.4, N_t = 0.2, N = 0.6, N_b = 0.8, \lambda = 0.4, K = 0.5, \beta = 0.2,$ and $\varepsilon = 0.2$

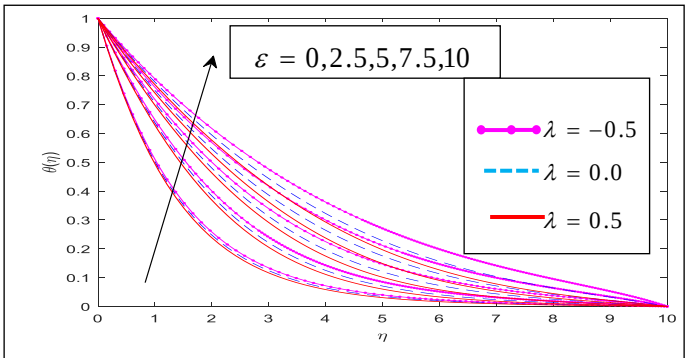

Fig.10:Temperature profile for different values of ε and λ at $E_c = 0.02, L_e = 0.62, R = 0.2, P_r = 0.72, R_d = 1.2, A = 0.5, M = 0.4, N_t = 0.2, N = 0.6, N_b = 0.8, Q = 0.2, K = 0.5, \xi = 0.8,$ and $\beta = 0.2$

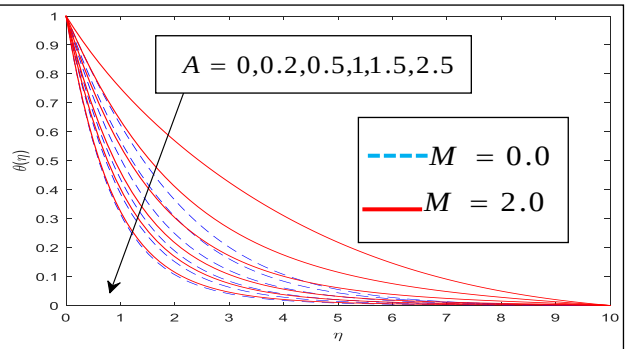

Fig.11:Temperature profile for different values of A and M at $E_c = 0.02, L_e = 0.62, R = 0.2, P_r = 0.72, Q = 0.2, \lambda = 0.4, \beta = 0.2,$ $N_t = 0.2, N = 0.6, N_b = 0.8, R_d = 1.2, K = 0.5, \xi = 0.8,$ and $\varepsilon = 0.2$

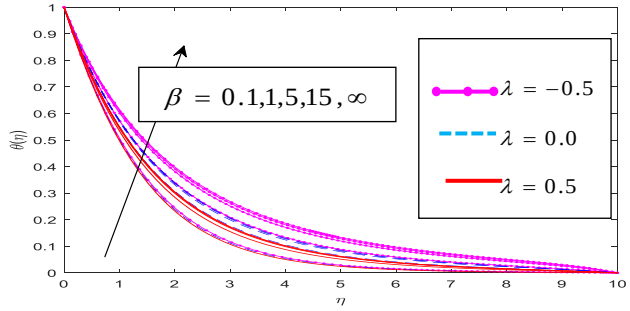

Fig. 12:Temperature profile for different values of β and λ at $E_c = 0.02, L_e = 0.62, R = 0.2, P_r = 0.72, Q = 0.2, A = 0.5, M = 0.4,$ $N_t = 0.2, N = 0.6, N_b = 0.8, R_d = 1.2, K = 0.5, \xi = 0.8,$ and $\varepsilon = 0.2$

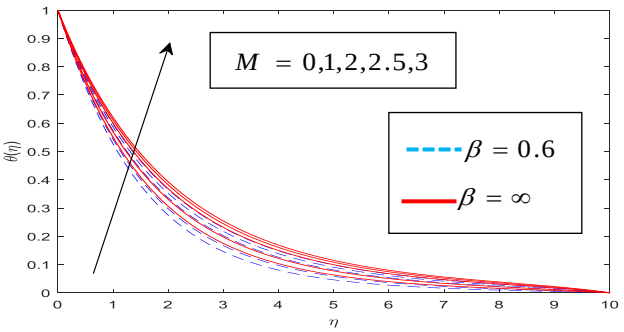

Fig. 13:Temperature profile for different values of M and A at $E_c = 0.02, L_e = 0.62, R = 0.2, P_r = 0.72, Q = 0.2, \lambda = 0.4, A = 0.5, N_t = 0.2,$ $N = 0.6, N_b = 0.8, R_d = 1.2, K = 0.5, \xi = 0.8,$ and $\varepsilon = 0.2$

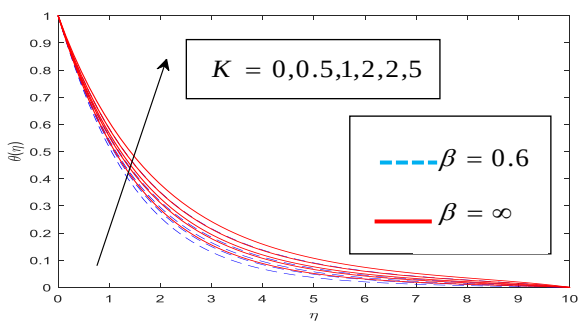

Fig. 14:Temperature profile for different values of K and A at $E_c = 0.02, L_e = 0.62, R = 0.2, P_r = 0.72, Q = 0.2, \lambda = 0.4, M = 0.4,$ $N_t = 0.2, N = 0.6, N_b = 0.8, R_d = 1.2, A = 0.5, \xi = 0.8,$ and

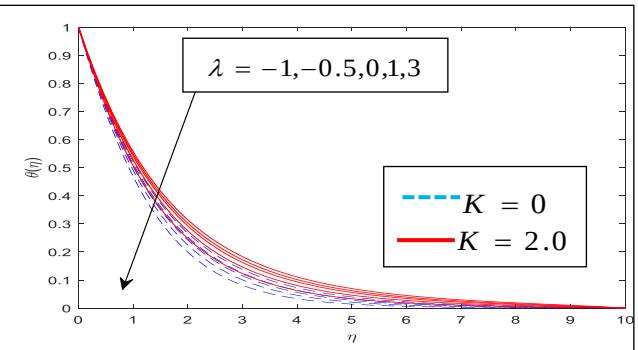

Fig. 15:Temperature profile for different values of λ and K at $E_c = 0.02, L_e = 0.62, R = 0.2, P_r = 0.72, Q = 0.2, \beta = 0.2, M = 0.4,$ $N_t = 0.2, N = 0.6, N_b = 0.8, R_d = 1.2, \lambda = 0.4, \xi = 0.8,$ and $\varepsilon = 0.2$

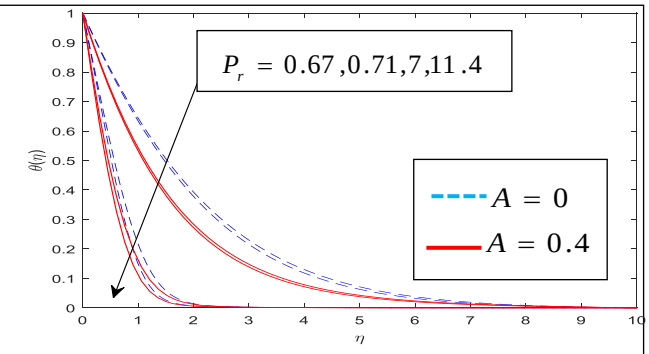

Fig. 16:Temperature profile for different values of P_r and A at $E_c = 0.02, L_e = 0.62, R = 0.2, \beta = 0.2, Q = 0.2, \lambda = 0.4, M = 0.4,$ $N_t = 0.2, N = 0.6, N_b = 0.8, R_d = 1.2, K = 0.5, \xi = 0.8,$ and $\varepsilon = 0.2$

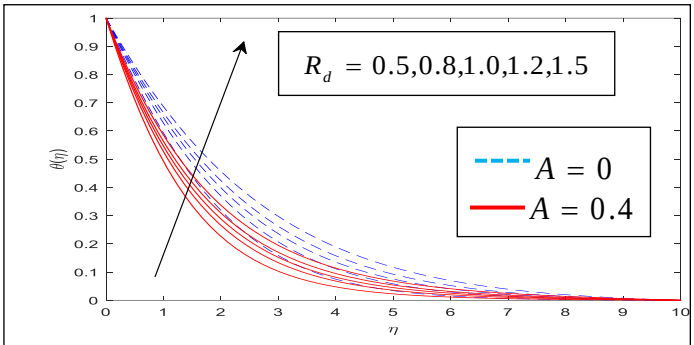

Fig.17:Temperature profile for different values of R_d and A at $E_c = 0.02, L_e = 0.62, R = 0.2, P_r = 0.72, Q = 0.2, \beta = 0.2, M = 0.4,$ $N_t = 0.2, N = 0.6, N_b = 0.8, \lambda = 0.4, K = 0.5, \xi = 0.8,$ and $\varepsilon = 0.2$

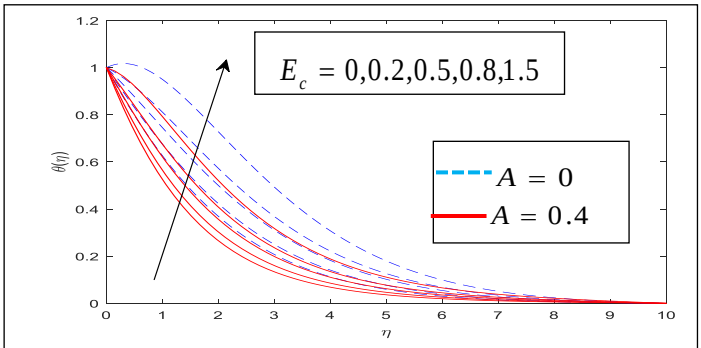

Fig.18:Temperature profile for different values of E_c and A at $\lambda = 0.4, L_e = 0.62, R = 0.2, P_r = 0.72, Q = 0.2, \beta = 0.2, M = 0.4,$ $N_t = 0.2, N = 0.6, N_b = 0.8, R_d = 1.2K = 0.5, \xi = 0.8,$ and $\varepsilon = 0.2$

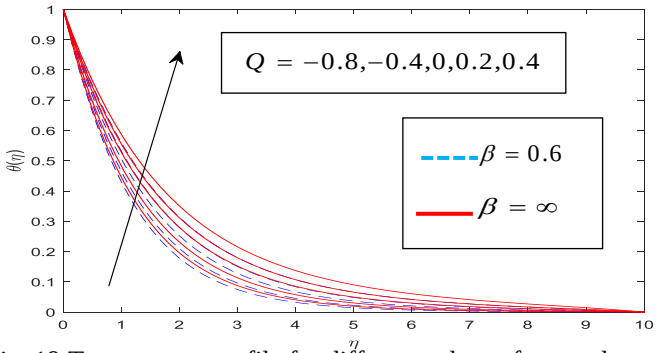

Fig. 19:Temperature profile for different values of Q and A at $E_c = 0.02, L_e = 0.62, R = 0.2, P_r = 0.72, R_d = 1.2, A = 0.5, M = 0.4,$ $N_t = 0.2, N = 0.6, N_b = 0.8, \lambda = 0.4, K = 0.5, \xi = 0.8,$ and $\varepsilon = 0.2$

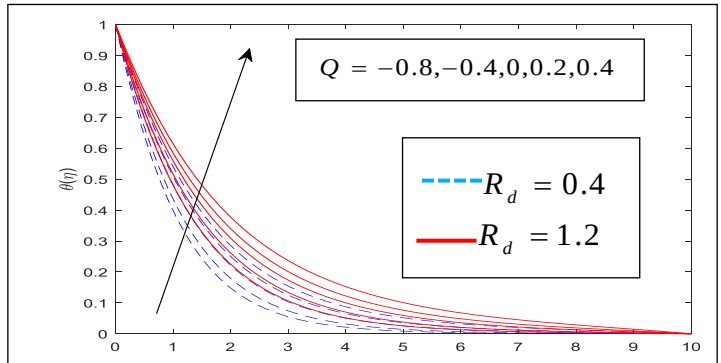

Fig. 20:Temperature profile for different values of Q and R_d at $E_c = 0.02, L_e = 0.62, R = 0.2, P_r = 0.72, A = 0.5, \beta = 0.2, M = 0.4,$ $N_t = 0.2, N = 0.6, N_b = 0.8, \lambda = 0.4, K = 0.5, \xi = 0.8,$ and $\varepsilon = 0.2$

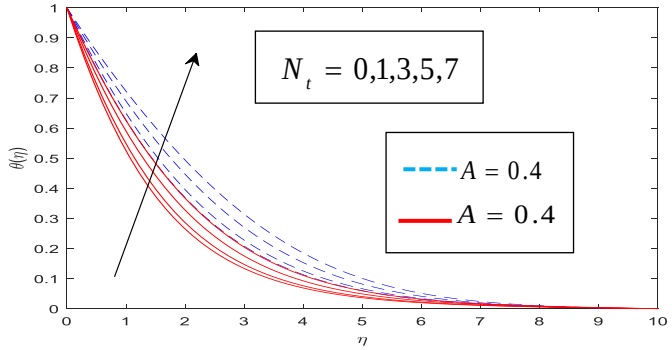

Fig. 21:Temperature profile for different values of N_t and A at $E_c = 0.02, L_e = 0.62, R = 0.2, P_r = 0.72, R_d = 1.2, \beta = 0.2, M = 0.4,$ $Q = 0.2, N = 0.6, N_b = 0.8, \lambda = 0.4, K = 0.5, \xi = 0.8,$ and $\varepsilon = 0.2$

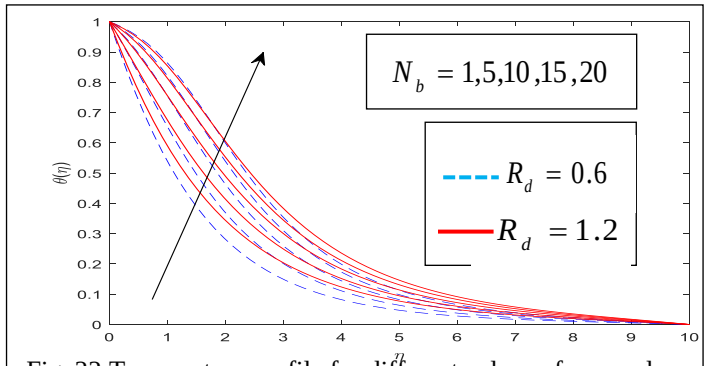

Fig. 22:Temperature profile for different values of N_b and R_d at $E_c = 0.02, L_e = 0.62, R = 0.2, P_r = 0.72, Q = 0.2, A = 0.5, M = 0.4,$ $N_t = 0.2, N = 0.6, \beta = 0.2, \lambda = 0.4, K = 0.5, \xi = 0.8,$ and $\varepsilon = 0.2$

Figs 9–22 demonstrate the physics of dimensionless temperature profile $(\theta(\eta))$ for different values of $\xi, \varepsilon, A, \beta, M, K, \lambda, P_r, R_d, E_c, Q, N_t$ and N_b .In Figs 9, effect of ξ on the thermal boundary layer for $A = 0$ (steady flow) and

$A = 0.4$ (unsteady flow) is shown. It can be seen that increase in ξ increases the temperature profile. Moreover, rise in the thermal boundary layer is pronounced for steady flow. An illustration of the effect of ε over temperature profile for all cases of λ is presented in Figs 10. It is noticed that an increase in the magnitude of ε leads to rise in the temperature profile significantly for higher values of λ . Fig 11 exhibits temperature profile for different values A when $M = 0$ and $M = 2$. The thermal boundary layer thinning as A increases. Effect of β on the fluid temperature for all the three cases of λ is presented in Fig 12 . It is clear that increase in β lead to higher temperature across the boundary region for all values of λ . Also, when $\lambda < 0$, the rise in the fluid temperature is most evident. Fig 13 presents the effect of temperature profile for various values of M when $\beta = 0.6$ (Casson fluid) and $\beta = \infty$ (Newtonian fluid). It is seen that increasing values of M slightly enhance the temperature for both fluids. This is because electromagnetic forces dominate viscous forces for higher values of M and it results in thickening thermal boundary layer. Fig 14 reveals the effect of K on thermal boundary layer for $\beta = 0.6$ (Casson fluid) and $\beta = \infty$ (Newtonian fluid). The temperature region is an increasing function of K for both fluids especially for Newtonian fluid. Fig 15 depicts the effect of buoyancy parameter λ on the temperature profile for $K = 0$ and $K = 2$. As λ increases, the thermal boundary layer reduces. This behaviour occurs because the buoyancy forces enhance temperature gradient which leads to the thermal boundary layer thinning. Fig 16 portrays the influence of P_r on temperature profile for both $A = 0$ (steady flow) and $A = 0.4$ (unsteady flow). According to the definition, Prandtl number is the ratio of momentum diffusivity to thermal diffusivity, that is, large values of P_r implies weaker thermal diffusivity which then thinning the thermal boundary layer. Furthermore, it is observed that the temperature reduces more significantly for higher values of P_r . In Fig 17, the effect of R_d on temperature profile for $A = 0$ (steady flow) and $A = 0.4$ (unsteady flow) is revealed. It is observed that larger values of R_d increase the temperature significantly with the enhancement more pronounce for the steady case. Actually, it is true owing to the fact that higher values of *Rd* lead to large radiation effect and thus enhancing the thickness of thermal boundary layer. Fig 18 illustrates the variation of temperature profile for various values of E_c when $A = 0$ (steady flow) and $A = 0.4$ (unsteady flow). It is noticed that the fluid temperature is higher for larger values of E_c most especially for steady case. The viscous dissipation generates heat due to frictional heating between the fluid particles and this extra heat thickening the thermal boundary layer. Fig 19 elucidates the effect of Q over temperature profile when $\beta = 0.6$ (Casson fluid) and $\beta = \infty$ (Newtonian fluid). It is noticed that higher values of Q enhance the temperature for both fluids, however, the influence is more pronounced for Newtonian fluid. Fig 20 examines the variation of temperature profile for various values of Q when $R_d = 0.4$ and $R_d = 1.2$. It can be easily noticed from this figure that temperature is higher for larger values of Q . It is seen that rise in R_d promotes fluid temperature drastically for larger values of Q . Further, graphical representation of the effect of N_t over temperature profile when $A = 0$ (steady flow) and $A = 0.4$ (unsteady flow)is presented in Fig 21. It is apparent that temperature is an increasing function of N_t for both fluids due to the fact that higher N_t corresponds to higher temperature differences and shear gradient. It is also found that increasing N_t support temperature rise in steady fluid better than unsteady. Fig 22 displays the effect of various values of N_b on the temperature profile for $R_d = 0.6$ and $R_d = 1.2$. An increase in N_b increases the thermal boundary layer due to the fact that increase in N_b implies higher diffusivity which leads to enhancement of fluid temperature.

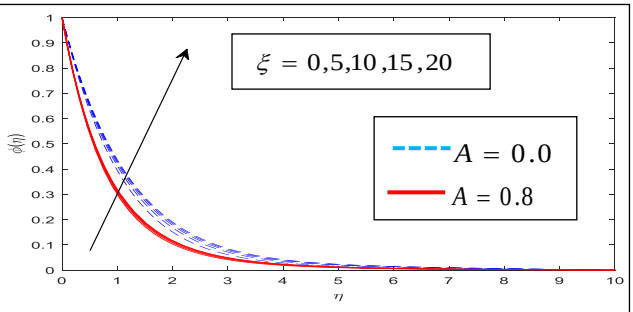

Fig.23:Concentration profile for different values of ξ and A at

$Q = 0.2, N = 0.6, N_b = 0.8, \lambda = 0.5, K = 0.5, \beta = 0.8,$ and $\varepsilon = 0.2$

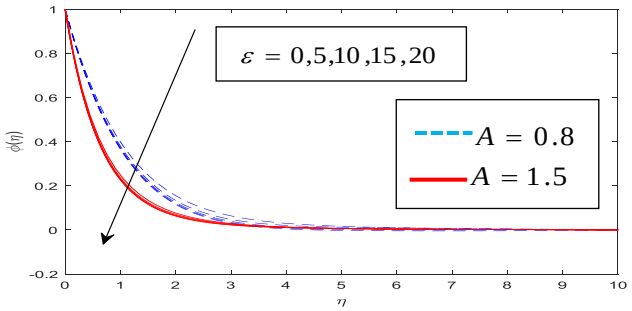

Fig.24:Concentration profile for different values of ε and ξ at

$E_c = 0.2, L_e = 0.62, R = 0.2, P_r = 0.72, R_d = 0.6, N_t = 0.2, M = 0.4,$

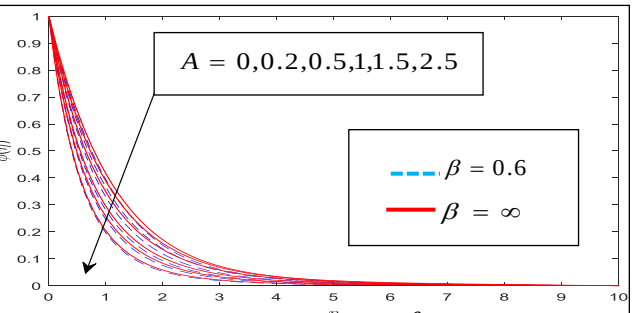

Fig. 25:Concentration profile for different values of A and β at

$E_c = 0.2, L_e = 0.62, R = 0.2, P_r = 0.72, R_d = 0.6, N_t = 0.2, M = 0.4,$

$Q = 0.2, N = 0.6, N_b = 0.8, \lambda = 0.5, K = 0.5, \xi = 0.8,$ and $\varepsilon = 0.2$

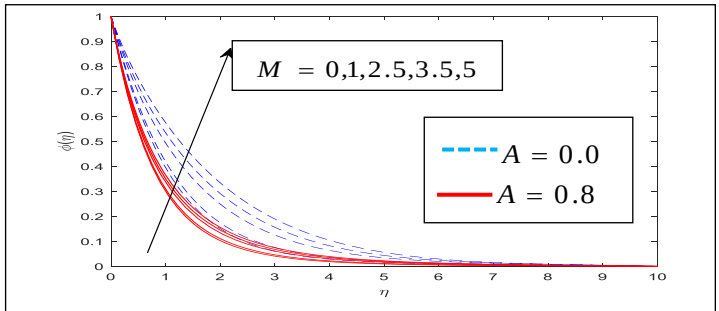

Fig. 26:Concentration profile for different values of M and A at

$E_c = 0.2, L_e = 0.62, R = 0.2, P_r = 0.72, R_d = 0.6, N_t = 0.2, \beta = 0.8,$

$Q = 0.2, N = 0.6, N_b = 0.8, \lambda = 0.5, K = 0.5, \xi = 0.8,$ and $\varepsilon = 0.2$

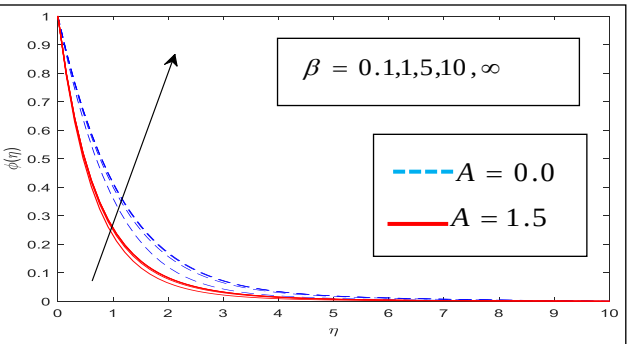

Fig. 27:Concentration profile for different values of β and A at

$E_c = 0.2, L_e = 0.62, R = 0.2, P_r = 0.72, R_d = 0.6, N_t = 0.2, M = 0.4,$

$Q = 0.2, N = 0.6, N_b = 0.8, \lambda = 0.5, K = 0.5, \xi = 0.8,$ and $\varepsilon = 0.2$

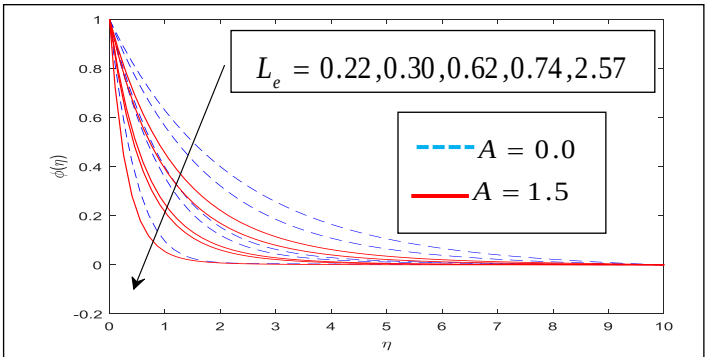

Fig. 28:Concentration profile for different values of L_e and A at

$E_c = 0.2, \beta = 0.8, R = 0.2, P_r = 0.72, R_d = 0.6, N_t = 0.2, M = 0.4,$

$Q = 0.2, N = 0.6, N_b = 0.8, \lambda = 0.5, K = 0.5, \xi = 0.8,$ and $\varepsilon = 0.2$

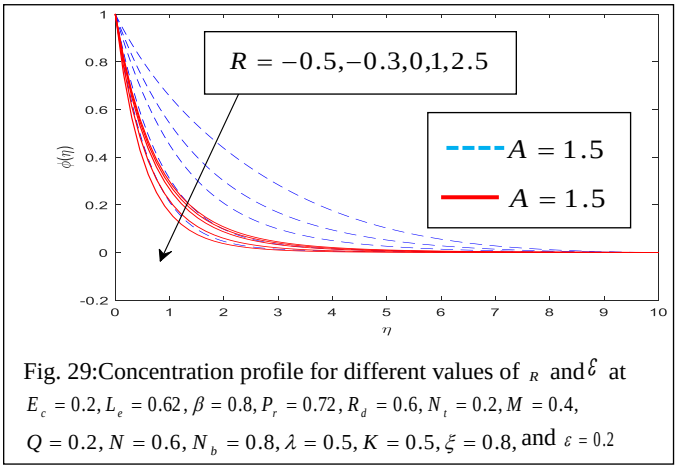

Fig. 29:Concentration profile for different values of R and ξ at $E_c = 0.2, L_e = 0.62, \beta = 0.8, P_r = 0.72, R_d = 0.6, N_t = 0.2, M = 0.4,$ $Q = 0.2, N = 0.6, N_b = 0.8, \lambda = 0.5, K = 0.5, \xi = 0.8,$ and $\varepsilon = 0.2$

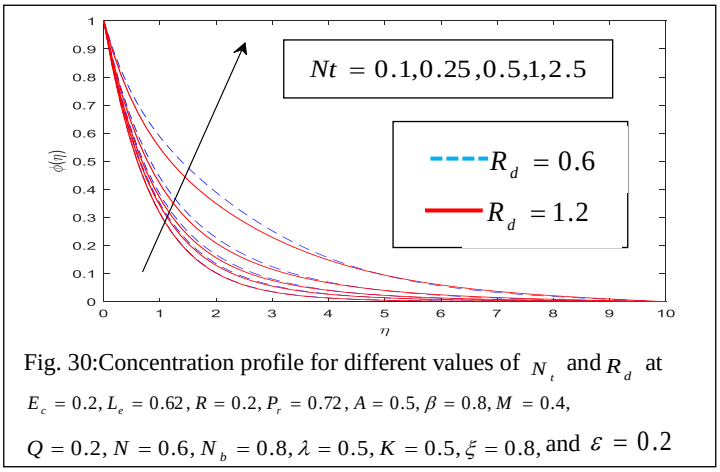

Fig. 30:Concentration profile for different values of N_t and R_d at $E_c = 0.2, L_e = 0.62, R = 0.2, P_r = 0.72, A = 0.5, \beta = 0.8, M = 0.4,$ $Q = 0.2, N = 0.6, N_b = 0.8, \lambda = 0.5, K = 0.5, \xi = 0.8,$ and $\varepsilon = 0.2$

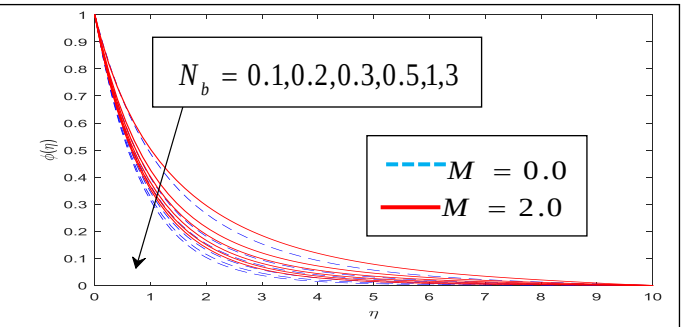

Fig. 31:Concentration profile for different values of N_b and M at $E_c = 0.2, L_e = 0.62, R = 0.2, P_r = 0.72, R_d = 0.6, N_t = 0.2, \beta = 0.8,$ $Q = 0.2, N = 0.6, A = 0.5, \lambda = 0.5, K = 0.5, \xi = 0.8,$ and $\varepsilon = 0.2$

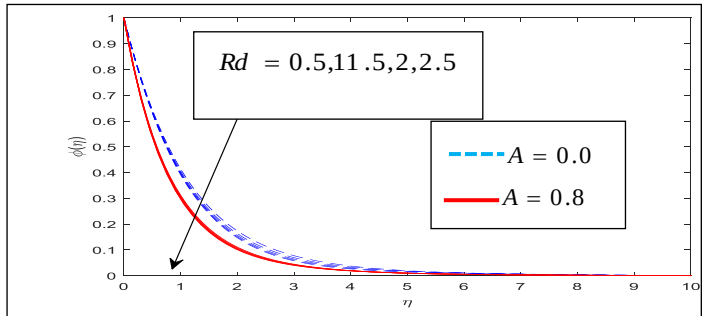

Fig. 32:Concentration profile for different values of R_d and A at $E_c = 0.2, L_e = 0.62, R = 0.2, P_r = 0.72, \beta = 0.8, N_t = 0.2, M = 0.4,$ $Q = 0.2, N = 0.6, N_b = 0.8, \lambda = 0.5, K = 0.5, \xi = 0.8,$ and $\varepsilon = 0.2$

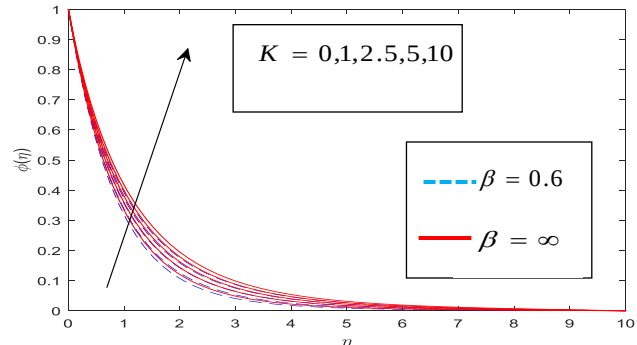

Fig. 33:Concentration profile for different values of K and A at $E_c = 0.2, L_e = 0.62, R = 0.2, P_r = 0.72, R_d = 0.6, N_t = 0.2, M = 0.4,$ $Q = 0.2, N = 0.6, N_b = 0.8, \lambda = 0.5, A = 0.5, \xi = 0.8,$ and $\varepsilon = 0.2$

Figs 23–33 present the variation of nanoparticle concentration profile ($\phi(\eta)$) for various values of $\xi, \varepsilon, A, M, \beta, L_e, R, N_t, N_b, R_d$ and K respectively. Fig 23 presents the effect of ξ on the nanoparticle concentration distribution when $A = 0$ (steady flow) and $A = 0.8$ (unsteady flow). It is noticeable that increase in ξ increases the concentration profile.

In addition, concentration boundary layer thickening is pronounced for steady flow. The variation of ε over nanoparticle concentration profile for $A = 0$ (steady flow) and $A = 1.5$ (unsteady flow) is portrayed in Figs 24. From the graph, it is deduced that concentration boundary layer thinning as ε rises with the effect more evident for unsteady flow. In Fig 25, the graphical representation of the effect of different values of A on nanoparticle concentration profile when $\beta = 0.6$ (Casson fluid) and $\beta = \infty$ (Newtonian fluid) is presented. It shows that increasing values of A efficiently reduces the concentration boundary layer thickness and also the that effect of *A* on concentration is more pronounced when $\beta = 0.6$ (for Casson fluid). Fig 26 displays the variation of M on nanoparticle concentration profile for $A = 0$ (steady flow) and $A = 0.8$ (unsteady flow). It is observed that higher values of M enhances nanoparticle concentration boundary layer thickness and is more noticeable when $A = 0$ (steady flow). The reason being that larger M strengthen the Lorentz force which is liable for decrease in the velocity and consequently thickening the nanoparticle concentration boundary layer. Fig 27 shows that nanoparticle concentration profile rises as β increases for both $A = 0$ (steady flow) and $A = 1.5$ (unsteady flow). It is also evident that the effect is more pronounced for steady flow. Fig 28 examines the influence of L_e (i.e. $L_e = 0.22, 0.30, 0.62, 0.74, 2.57$ for hydrogen, helium, water vapor, hydrogen sulphide and Propyl Benzene) on nanoparticle concentration profile when $A = 0$ (steady flow) and $A = 1.5$ (unsteady flow). It is inferred that in both cases, the concentration boundary layer thinning with increase in L_e. The variation of R against the nanoparticle concentration profile for both $A = 0$ (steady flow) and $A = 1.5$ (unsteady flow) in Fig 29 shows that concentration distribution decreases for increasing values of R . In Fig 30, effect of nanoparticle concentration profile for different value of N_t when $R_d = 0.1$ and $R_d = 0.6$ is displayed. From this figure, it is noticeably that increasing values of N_t effectively enhances the concentration boundary layer thickness. Furthermore, Fig 31 portrays the influence of N_b on nanoparticle concentration distribution when $M = 0$ and $M = 2$. It reveals that nanoparticle concentration decreases as N_b increases. In Fig 32, the variation of R_d on nanoparticle concentration profile for $A = 0$ (steady flow) and $A = 0.8$ (unsteady flow) is discussed. The graphical representation shows that nanoparticle concentration slightly reduces with increase in R_d. Effect of K on nanoparticle concentration profile for $\beta = 0.6$ (Casson fluid) and $\beta = \infty$ (Newtonian fluid) is illustrated in Fig 33. It is observed that concentration boundary layer thickening as K increases in both fluids, however, the effect of K on nanoparticle concentration is more significant when $\beta = \infty$ (Newtonian fluid).

Conclusion

The problem of MHD boundary layer flow of Casson fluid past an unsteady linearly stretching sheet through porous medium under the influence of variable thermo-physical property and nanoparticles has been studied. Influence of pertinent physical parameters on fluid profile and on the shear stress, heat and mass transfer rates at the porous wall are explained in detail. Numerical investigation of the present study reveals some of the following:

i. Higher values of variable plastic dynamic viscosity parameter ξ , Casson fluid parameter β , porosity parameter K , or magnetic parameter M reduces both the skin friction, local Nusselt number and Sherwood number.
ii. Increasing values of thermal buoyancy parameter λ enhances skin friction, local Nusselt number and Sherwood number respectively.
iii. Shear stress and mass transfer rates are enhanced by variable thermal conductivity parameter ε or diffusion parameter N_b , while heat transfer rate is drastically reduced with increasing values of variable thermal conductivity parameter ε or diffusion parameter N_b
iv. Local unsteadiness parameter A , when increases reduces skin friction but enhances both the local Nusselt number and Sherwood number.
v. As variable plastic dynamic viscosity parameter ξ increases, the fluid temperature and nanoparticle concentration distribution rises while the flow profile reduces.

vi. The fluid velocity and temperature boundary layer thickness enhance with increase in variable thermal conductivity whereas the nanoparticle concentration boundary layer becomes thinning

vii. Higher values of Casson fluid parameter β reduces the fluid velocity but enhances temperature and nanoparticle concentration of the fluid.

viii. The fluid velocity, temperature and nanoparticle concentration boundary layer become thinner for increasing values of the local unsteadiness parameter A .

ix. Increasing values of K reduces the fluid velocity profile whereas increasing both the thermal and nanoparticle concentration distribution.

x. Temperature and nanoparticle concentration boundary layer of the fluid becomes thicker as thermophoretic parameter N_t increases.

xi. Addition of diffusion parameter N_b^* or radiation parameter R_d to the fluid sufficiently enhances the temperature distribution however reduces nanoparticle concentration distribution.

References

[1] Sakiadis B. Boundarylayer behavior on continuous solid surfaces: I. Boundary layer equations for two dimensional and axisymmetric flow. AIChE J. 1961; 26-28. doi: 10.1002/aic.690070108

[2] Kumaran V, Ramanaiah G. A note on the flow over a stretching sheet. Acta Mech. 1996; 116: 229-233. doi: 10.1007/BF01171433

[3] Kechil SA, Hashim I. Flow and diffusion of chemically reactive species over a nonlinearly stretching sheet immersed in a porous medium. J Porous Media. 2009; 12: 1053-1063. doi: 10.1016/j.jmaa.2005.06.095

[4] Magyari E, Keller B. Heat and mass transfer in the boundary layers on an exponentially stretching continuous surface. J Phys D Appl Phys. 1999; 32: 577-585. doi: 10.1088/0022-3727/32/5/012

[5] Pramanik S. Casson fluid flow and heat transfer past an exponentially porous stretching surface in presence of thermal radiation. Ain Shams Eng J. Faculty of Engineering, Ain Shams University; 2014; 5:205-212. doi: 10.1016/j.asej.2013.05.003

[6] Cortell R. Viscous flow and heat transfer over a nonlinearly stretching sheet. Appl Math Comput. 2007;184: 864-873. doi: 10.1016/j.amc.2006.06.077

[7] Hsiao K. Mixed Convection with Radiation Effect over a Nonlinearly Stretching Sheet. World Acad Sci Eng Technol. 2010; 4: 338-342.

[8] Jat RN, Chand G, Rajotia D. MHD Heat and Mass Transfer for Viscous flow over Nonlinearly Stretching Sheet in a Porous Medium. Therm Energy Power Eng. 2014; 3: 191-197.

[9] Pop I, Na T-Y. Unsteady flow past a stretching sheet. Mech Res Commun. 1996; 23: 413-422. doi: 10.1016/0093-6413(96)00040-7

[10] Sharidan S, Mahmood T, Pop I. Similiarity solutions for the unsteady boundary layer flow and heat transfer due to a stretching sheet. Int J Appl Mech Eng. 2006; 11: 647-654.

[11] Mukhopadhyay S. Effect of thermal radiation on unsteady mixed convection flow and heat transfer over a porous stretching surface in porous medium. Int J Heat Mass Transf. Elsevier Ltd; 2009; 52:3261-3265. doi: 10.1016/j.ijheatmasstransfer.2008.12.029

[12] Chamkha A, Aly A, Mansour M. Similarity solution for unsteady heat and mass transfer from a stretching surface embedded in a porous medium with suction/injection and chemical reaction effects. Chem Eng Comm. 2010; 197: 846-858. doi: 10.1080/00986440903359087

[13] Bhattacharyya K, Mukhopadhyay S, Layek GC. Slip effects on an unsteady boundary layer stagnation point flow and heat transfer towards a stretching sheet. Chinese Phys Lett. 2011; 28: 094702. doi: 10.1016/j.ijheatmasstransfer.2010.09.041

[14] Takhar HS, Chamkha AJ, Nath G. Flow and mass transfer on a stretching sheet with a magnetic field and chemically reactive species. Int J Eng Sci. 2000; 38: 1303-1314.

[15] Hsiao KL. MHD mixed convection for viscoelastic fluid past a porous wedge. Int J Non Linear Mech. Elsevier; 2011; 46: 1-8. doi: 10.1016/j.ijnonlinmec.2010.06.005

[16] Aurangzaib, Kasim ARM, Mohammad NF, Shafie S. Effect of thermal stratification on MHD free convection with heat and mass transfer over an unsteady stretching surface with heat source, Hall current and chemical reaction. Int J Adv Eng Sci Appl Math. 2012; 4: 217-225. doi: 10.1007/s12572-012-0066-y

[17] Bhattacharyya K, Mukhopadhyay S, Layek GC. Unsteady MHD boundary layer flow with diffusion and first-order chemical reaction over a permeable stretching sheet with suction or blowing. Chem Eng Comm. 2013; 200: 379-397. doi:10.1080/00986445.2012.712577

[18] Seini IY, Makinde DO. Boundary layer flow near stagnation-points on a vertical surface with slip in the presence of transverse magnetic field. Int J Numer Methods Heat Fluid Flow. 2014; 24: 643-653. doi:10.1108/HFF-04-2012-0094

[19] Mabood F, Khan WA, Ismail AIM. MHD stagnation point flow and heat transfer impinging on stretching sheet with chemical reaction and transpiration. Chem Eng J. Elsevier B.V.; 2015; 273: 430-437. doi:10.1016/j.cej.2015.03.037

[20] Khan U, Ahmed N, Mohyud-Din ST. Heat transfer effects on carbon nanotubes suspended nanofluid flow in a channel with non-parallel walls under the effect of velocity slip boundary condition: a numerical study. Neural Comput Appl. Springer London; 2015; doi: 10.1007/s00521-015-2035-4

[21] Mohyud-Din ST, Zaidi ZA, Khan U, Ahmed N. On heat and mass transfer analysis for the flow of a nanofluid between rotating parallel plates. Aerosp Sci Technol. 2015; 46: 514-522. doi: 10.1007/s40819-015-0032-z

[22] Mohyud-Din S, Khan U, Ahmed N, Hassan S. Magnetohydrodynamic Flow and Heat Transfer of Nanofluids in Stretchable Convergent/Divergent Channels. Appl Sci. 2015; 5: 1639-1664. doi: 10.3390/app5041639

[23] Khan WA, Makinde OD, Khan ZH. Non-aligned MHD stagnation point flow of variable viscosity nanofluids past a stretching sheet with radiative heat. Int J Heat Mass Transf. Elsevier Ltd; 2016; 96: 525-534. doi: 10.1016/j.ijheatmasstransfer.2016.01.052

[24] Khan U, Ahmed N, Mohyud-Din ST. Thermo-diffusion, diffusion-thermo and chemical reaction effects on MHD flow of viscous fluid in divergent and convergent channels. Chem Eng Sci. Elsevier; 2016; 141:17-27. doi: 10.1016/j.ces.2015.10.032

[25] Mohyud-Din ST, Ahmed N, Khan U, Waheed A, Hussain S, Darus M. On Combined Effects of Heat Transfer and Chemical Reaction for the Flow through an Asymmetric Channel with Orthogonally Deformable Porous Walls. Math Probl Eng. 2016; 2016.
doi: 10.1155/2016/2568785

[26] Mohyud-Din ST, Jan SU, Khan U, Ahmed N. MHD flow of radiative micropolar nanofluid in a porous channel: optimal and numerical solutions. Neural Comput Appl. Springer London; 2016; 1-9. doi: 10.1007/s00521-016-2493-3

[27] Casson N. A flow equation for pigment-oil suspensions of the printing ink type. Mill CC, Ed, Rheol Disperse Syst Pergamon Press Oxford. In: Mill,. Rheology of Disperse Systems, Pergamon Press, Oxford; 1959; 84-104.

[28] Mukhopadhyay S. Effects of thermal radiation on Casson fluid flow and heat transfer over an unsteady stretching surface subjected to suction/blowing. Chinese Phys B. 2013; 22: 114702. doi: 10.1088/1674-1056/22/11/114702

[29] Nadeem S, Haq RU, Akbar NS, Khan ZH. MHD three-dimensional Casson fluid flow past a porous linearly stretching sheet. Alexandria Eng J. Faculty of Engineering, Alexandria University; 2013; 52: 577-582. doi: 10.1016/j.aej.2013.08.005

[30] Ibrahim W, Makinde OD. Magnetohydrodynamic stagnation point flow and heat transfer of Casson nanofluid past a stretching sheet with slip and convective boundary condition,. J Aerosp Eng. 2015; 29:04015037. doi: 10.1061/(ASCE)AS.1943-5525.0000529

[31] Benazir J., Sivaraj A, Makinde OD. Unsteady magnetohydrodynamic Casson fluid flow over a vertical cone and flat plate with non-uniform heat source/sink. Int J Eng Res Africa. 2016; 21: 69-83.

[32] Oyelakin IS, Mondal S, Sibanda P. Unsteady Casson nanofluid flow over a stretching sheet with thermal radiation, convective and slip boundary conditions. Alexandria Eng J. Faculty of Engineering, Alexandria University; 2016; 55: 1025-1035.
doi: 10.1016/j.aej.2016.03.003

[33] Ullah I, Bhattacharyya K, Shafie S, Khan I, (2016) Unsteady MHD Mixed Convection Slip Flow of Casson Fluid over Nonlinearly Stretching Sheet Embedded in a Porous Medium with Chemical Reaction, Thermal Radiation, Heat Generation/Absorption and Convective Boundary Conditions. PLoS ONE 11(10): e0165348. doi:10.1371/journal.pone.0165348

[34] Sogbetun L.O., Fasasi Y.A., Akinosho G.A., Azeez S.O. (2018) MHD Nonlinear Convective Flow of Casson Fluid with Variable Thermo-Physical Property and Nanoparticles along an Exponentially Stretching Sheet with Suction and Exponentially Decaying Internal Heat Generation. American Journal of Applied and Industrial Science and Engineering. doi: GBrainV1N1AJAIC2018AAA.

[35] Gilbert Makanda, Sachin Shaw, and Precious Sibanda (2014) Diffusion of Chemically Reactive Species in Casson Fluid Flow over an Unsteady Stretching Surface in Porous Medium in the Presence of a Magnetic Field. Hindawi Publishing Corporation Mathematical Problems in Engineering Volume 2015, Article ID 724596, 10 pages, http://dx.doi.org/10.1155/2015/724596

[36] Raptis A. Radiation and free convection flow through a Porous medium. Int Commun Heat Mass Transfer 1998;25:289–95. Journal of Results in Physics, 7 (2017) 2124-2133, http://dx.doi.org/10.1016/j.rinp.2017.06.010.

[37] Sparrow EM, Cess RD. Radiation heat transfer. Washington, DC: Augmented edition Hemisphere Publ. Crop; 1978 [chapters 7 and 10].

[38] Animasaun I.L., Adebile E.A., Fagbade A.I.(2015) Casson fluid flow with variable thermo-physical property along exponentially stretching sheet with suction and exponentially decaying internal heat generation using the homotopy analysis method Journal of the Nigeria Mathematical Society, http://dx.doi.org/10.1016/j.jnnms.2015.02.001

[39] Imran Ullah, Krishnendu Bhattacharyya, Sharidan Shafie1, Ilyas Khan (2016) Unsteady MHD Mixed Convection Slip Flow of Casson Fluid over Nonlinearly Stretching Sheet Embedded in a Porous Medium with Chemical Reaction, Thermal Radiation, Heat Generation/Absorption and Convective Boundary Conditions. Plos One 11(10) 1-35. doi:10.1371/journal.pone.0165348.